Analysis of the force-frequency characteristics of the resonant DETF beam with silts

Huichao Shi[1,a*], Xirui Kang[1,b], and Wenlong Li[2,c]

[1]College of Information Science and Technology, Beijing University of Chemical Technology Beijing, China

[2]North Automatic Control Technology Research Institute, Taiyuan, 003003, China

[a]shc321167@163.com, [b]2018310055@mail.buct.edu.cn, [c]dxybb123@163.com

[*]corresponding author

Keywords: resonant sensor; DETF; silt structure; natural frequency

Abstract: In this paper, the DETF with silt structure on the beam is designed and manufactured. The natural frequency of the DETF beam with silts is measured by loading different axial tensile displacement on the DETF beam. The force-frequency characteristics between the axial force and the natural frequency of the DETF beam with silts is obtained and compared with the theoretical results. The experimental results are in good agreement with the theoretical results.

1. Introduction

Resonant sensor has many advantages, such as high resolution, high stability, digital output and so on, and it has been widely used[1-4]. As the main component of the resonant sensor, the resonator determines the performance of the sensor. The existing resonator mainly include resonant beam, resonant cylinder, resonant diaphragm and so on[5-11], and the DETF (Double ended fixed tuning fork) structure is easy to process and is often used[10-11]. For these resonators, piezoresistive effect is often used to sensitize the local stress on the resonator to measure the vibration signal of the resonator[12-14]. Increasing the local stress of the resonator can increase the amplitude of the vibration signal, and increase the amplitude of the sensor output signal without introducing noise[15-18]. This is more meaningful for the resonant sensor with small structure size and weak output signal.

Based on the stress concentration effect of the silt structure, the silts can realize the stress amplification in the local region of resonant beam[19], so that the amplitude of the output resonant signal can be increased without increasing the excitation signal power. This method can improve the amplitude detection sensitivity of the resonator and the signal-to-noise ratio of the output signal[20]. However, due to the introduction of silt structure, the natural frequency of resonator is changed, and variation of natural frequency of resonator with axial force change is also affected.

In this paper, the silt structure on the DEFT beam is designed and manufactured. The natural frequency of the resonant beam is measured by loading different axial forces on the DETF beam. The relationship between the axial force and the natural frequency of the DETF beam is obtained and compared with the theoretical results.

2. Vibration characteristic equation of DETF beam with silts

The DETF resonator mainly consists of two identical resonant beams, as shown in Fig.1(a). When the DETF resonator is working, axial force along both beams of DETF caused by measured quantity changes the nature frequency of the DETF beams. Two beams of DETF resonator are vibrating with same frequency and opposite phase in the XY plane, and the stress and moment produced by each beam are equal in magnitude and opposite in direction in the combined place, when it working at the inverse vibration mode as shown in Fig.1(b). The natural frequency depends only on the geometric parameters of DETF resonator and the axial force along both beam caused by the measured quantity.

Copyright © (2018) Francis Academic Press, UK DOI: 10.25236/icbdai.2018.023

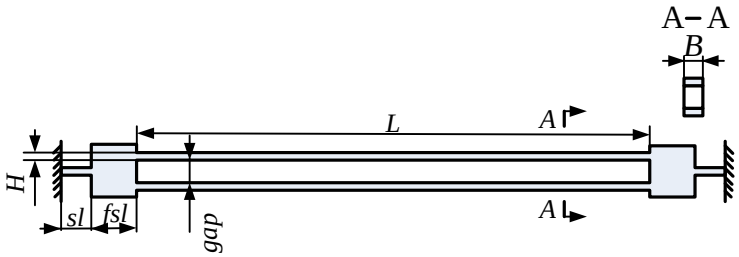

(a)

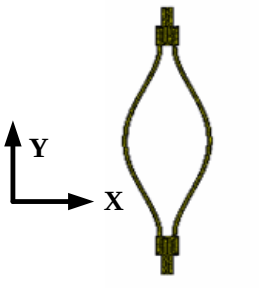

Working Mode

(b)

Fig. 1 (a) DETF resonators with boundary structures, (b) working mode shapes of DETF resonator

When the DETF resonator is working, the displacement of the fixed end is very small (almost zero). So the two beam of the DETF resonator can be regarded as independent double clamped resonant beam. According to the Euler-Bernoulli beam model, the differential equations of motion for the transverse bending vibration of beam is

$$\frac{\partial^2}{\partial x^2}\left(EI\frac{\partial^2 w(x,t)}{\partial x^2}\right)+\frac{\partial}{\partial x}\left(F\frac{\partial w(x,t)}{\partial x}\right)+\rho BH\frac{\partial^2 w(x,t)}{\partial t^2}=P(x) \tag{1}$$

Where, $w(x,t)$ is lateral displacement of a DETF beam, x is the distance along the DETF beam from a clamped end, and t is time. B is width of the DETF beam, and H is thickness of the DETF beam. ρ is material density, and E is Young's modulus of the DETF material. I is the second moment of DETF beam cross section. F is the axial force along both beam of DETF caused by measured quantity， $P(x)$ is excitation force taking the DETF beam into vibration state.

Boundary conditions of this clamped-clamped DETF beam are

$$w(0,t)=w(L,t)=0 \qquad \left.\frac{\partial w}{\partial x}\right|_{x=0}=\left.\frac{\partial w}{\partial x}\right|_{x=L}=0 \tag{2}$$

Where, L is length of the DETF beam.

Since the natural frequency is the inherent property of the DETF beam, it only depends on the equivalent stiffness and equivalent mass of the DETF beam. So the natural frequency is

$$\omega_n=\left(\frac{\int_L \frac{EH^3}{12}B(W''(x))^2dx-\int_L NW''(x)W(x)dx}{\int_L \rho HBW^2(x)dx}\right)^{\frac{1}{2}} \tag{3}$$

Classical mode function given by Bishop and Jobnson[21] is used as the first order linear undamped mode function of the DETF beam $W(x)$. When the DETF beam has two silt structures, the cross-sectional area of the beam changes. The structure sketch of the silt-beam is given as Fig. 2.

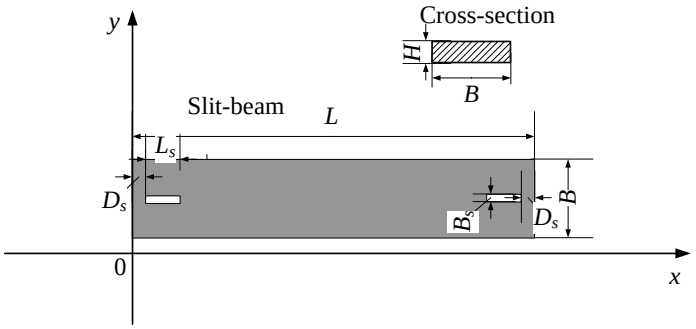

Fig.2 Schematic of the slit-beam of the DETF

Shi et al. (2013) using step function $u(x)$ to describe the width $B(x)$ of the DETF beam with slits in the axial direction along *x*, and established a model of the slit-beam in line with Euler-Bernoulli beam modeling when consider the external forces and moments.

The natural frequency is only determined by the ratio of the equivalent stiffness and equivalent mass of the system itself. The cross-sectional area of the DETF beam is changing along axial direction due to the slits, which cause the equivalent stiffness and equivalent mass of the DETF beam to change. The proration method[20, 22, 23] is used to calculate the natural frequency of slit-beam of the DETF, and the natural frequency of the DETF beam with slits are

$$\omega_{slit} = \left(\frac{\sum_{i=1}^{n} \left(\int_{L_i} \frac{EH^3}{12} B_i(x)(W''(x))^2 dx - \int_{L_i} NW''(x)W(x)dx \right)}{\sum_{i=1}^{n} \int_{L_i} \rho H B_i(x) W^2(x) dx} \right)^{\frac{1}{2}} \tag{4}$$

Based on the above equations, the results of theoretical calculation can be given by calculation in Fig. 3 and Fig. 4, respectively. A group of parameters are used: *L*=40mm, *B*=5mm, *H*=0.3mm, *gap*=9.4mm, *fsl*=5mm, *sl*=8mm , and the Young's modulus of the DETF material $E = 206$ GPa , the material density of DETF ρ=7650 Kg m^{-3}.

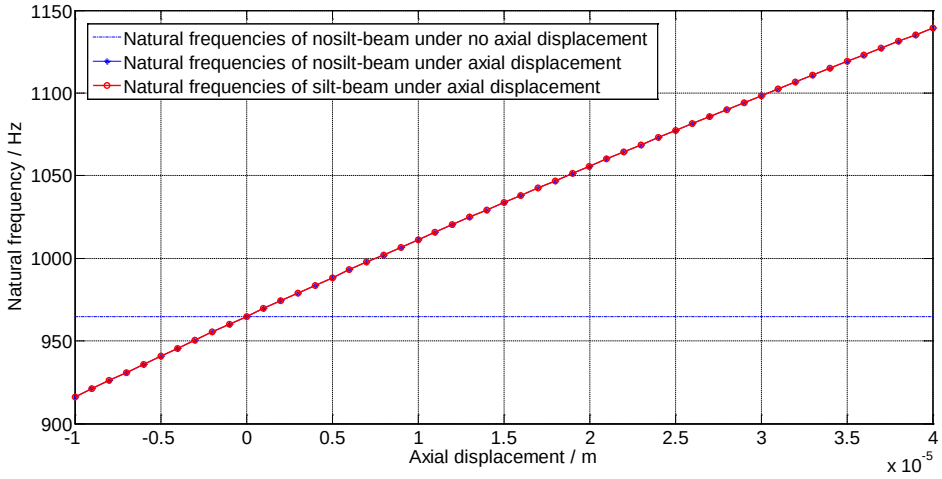

Fig.3 Theoretical calculation of the force-frequency characteristics when L_s=0mm, B_s=0mm, D_s=0mm.

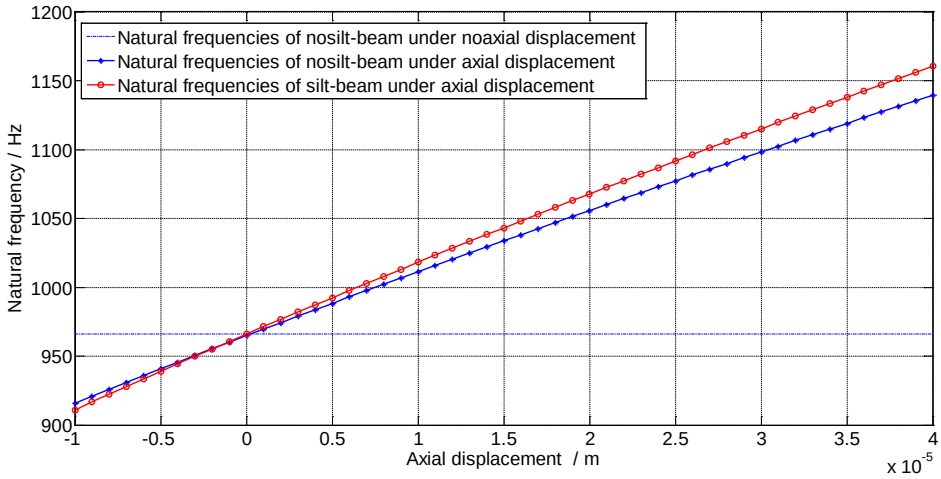

Fig.4 Theoretical calculation of the force-frequency characteristics when L_s=1.2mm, B_s=1.2mm, D_s=2mm.

It can be found from Fig.3 that when the silt length, silt width and the distance of silt from the clamped end are zero, the natural frequencies of the DETF beam calculated respectively by Eq.(3) and Eq.(4) are same. When there is a silt structure on the beam, the difference of the natural frequencies between silt beam and no-silt beam increases with the increase of the axial force of the DETF beam. It can be seen from Fig. 4 that the silt structure changes the changing trend of the resonant beam with the change of the axial force, and makes the natural frequency of the DETF beam become larger.

3. Experiment and analysis

In order to validate the above theoretical calculation model, the DEFT beam with silts is processed. Manganese steel is used for machining the DEFT beam. The sizes of the silt-beam is L=40mm, B=5mm, H=0.3mm, L_s=1.2mm, B_s=1.2mm, D_s=2mm. In order to measure the natural frequency of the DEFT beam with silts and the natural frequencies of the DEFT beam with silts under different axial loads, the experimental platform fixing the DEFT beam is processed and the axial force is loaded in the form of displacement. The photos of the DEFT beam with silts and the experimental platform are shown in Fig. 5. On the experimental platform, axial force of the DEFT beam are loaded in the form of displacement. Measuring rod of screw micrometer is used to realizing axial tensile displacement, and tensile displacement can be accurate to 10 microns. The natural frequencies of DEFT beam with silts are measured by laser vibrometer after tapping the structure of DEFT beam to make it in free vibration state.

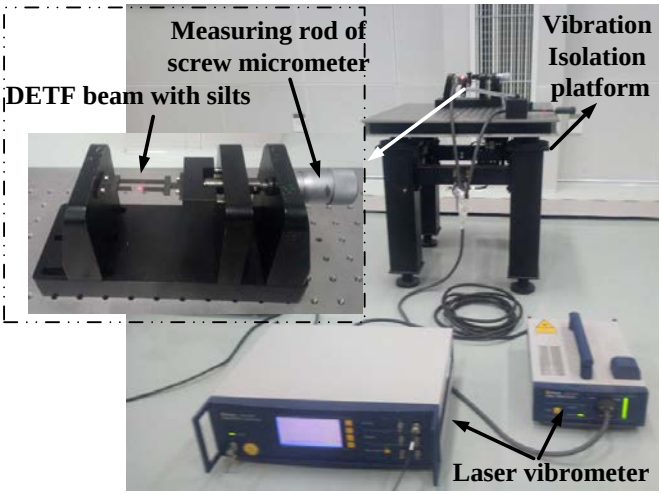

Fig.5 Photos of the DEFT beam with silts and the experimental platform.

Comparison of the calculated results of theoretical model with the results of experiment are given in Fig. 6 and Fig. 7, respectively. It can be seen that in Fig. 6 and Fig. 7, the trend of theoretical calculation is consistent well with that of experimental results. However, there are some differences between the theoretical results and the experimental results both when there is silts and there is not silts. The difference may be caused by the insufficient boundary conditions and machining accuracy.

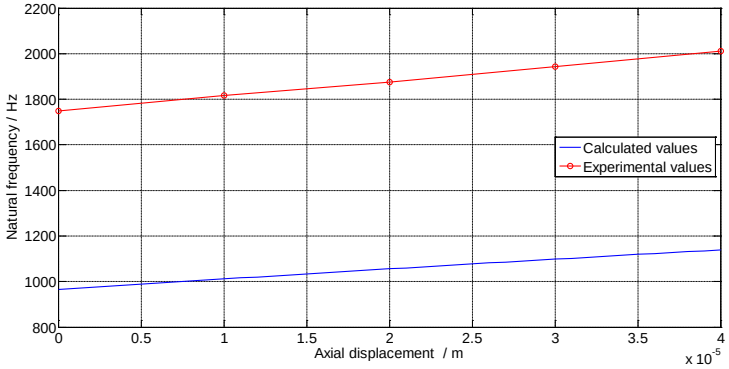

Fig.6 Comparison of the theoretical results with the experiment results of the force-frequency characteristics when L_s=0mm, B_s=0mm, D_s=0mm.

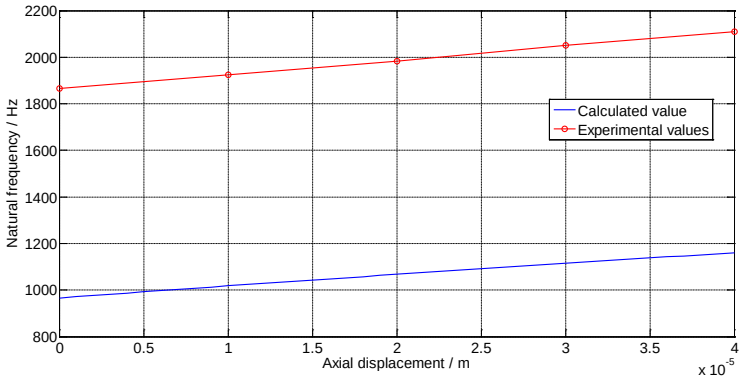

Fig.7 Comparison of the theoretical results with the experiment results of the force-frequency characteristics when L_s=1.2mm, B_s=1.2mm, D_s=2mm.

4. Conclusion

In this paper, the DETF with silt structure on the beam is designed and manufactured. The natural frequency of the DETF beam with silts is measured by loading different axial tensile displacement on the DETF beam. The force-frequency characteristics between the axial force and the natural frequency of the DETF beam with silts is obtained by experiment and compared with the theoretical results. By comparison, it can be found that the experimental results are in good agreement with the theoretical results.

Acknowledgement

This study is supported by the Fundamental Research Funds for the Central Universities (ZY1838).

References

[1] Greenwood J.C., Wray T. (1993) High accuracy pressure measurement with a silicon resonant sensor. Sensors and Actuators A: Physical 37-38:82-85.

[2] Kyoichi I., Hideki K., Takashi K., et al. (1990) Silicon pressure sensor integrates resonant strain

gauge on diaphragm. Sensors and Actuators A: Physical 21:146-150.

[3] Tang, Z.Y., Xing, W.W., Guo, Z.S., Zhang, Z. (2011) An electrothermally excited dual beams silicon resonant pressure sensor with temperature compensation. Microsyst. Technol. 17 1481-1490.

[4] Li, Q.F., Fan, S.C., Tang, Z.Y., Xing, W.W., (2012) Non-linear dynamics of an electrothermally excited resonant pressure sensor. Sens. Actuator A: Phys. 188 15-28

[5] Stemme Goran, (1991) Resonant silicon sensors. Micromech. Microeng, 1: 113-125

[6] Smiths J.G., Tilmans H.A.C., Hoen K., et al. (1983) Resonant diaphragm pressure measurement system with ZnO on Si excitation. Sensors and Actuators A, 4: 565-571

[7] Greenwood J.C. (1988)Miniature silicon resonant pressure sensor. Control Theory and Applications, IEE Proceedings D, 1988, 135(5): 369-372

[8] Burns D.W., Zook J.D., Horning R.D., et al. (1995) Sealed-cavity resonant microbeam pressure sensor. Sensors and Actuators A, 48(3): 179-186

[9] Ferrari V., Ghisla A., Marioli D., Taroni A. (2005) Silicon resonant accelerometer with electronic compensation of input-output cross-talk. Sensors and Actuators A: Physical 123-124:258-266.

[10] Hopkins R., Miola J., Setterlund R., et al. (2006) The Silicon Oscillating Accelerometer: A High Performance MEMS Accelerometer for Precision Navigation and Strategic Guidance Applications. The Draper Technology Digest 10: 4-13.

[11] Lee J.E.Y., Bahreyni B., Seshia A.A., (2008) An Axial Strain Modulated Double-ended Tuning Fork Electrometer. Sensors and Actuators A:Physical 148:395-400.

[12] Bashir R., Gupta A., Neudeck G.W., McElfresh M., et al. (2000) On the design of piezoresistive silicon cantilevers with stress conceniration regions (SCR) for scanning Probe microscopy applications. Micromech. Microeng.,10:483-491

[13] Ahmed A.S. Mohammed, Walied A., et al. (2010) Optimization of geometric Characteristics to improve sensing performance of MEMS Piezoresistive strain sensor. Micromech.Microeng. 20:015015

[14] Harley J.A., Kenny T.W. (2000) l/f Noise Considerations for the Design and Process Optimization of Piezoresistive Cantilevers. Journal of Microelectromechanical Systems, 9:226-235

[15] Bashir R., Gupta A., Neudeck G.W., et al. (2000) On the design of piezoresistive silicon cantilevers with stress conceniration regions (SCR) for scanning Probe microscopy applications. Micromech. Microeng., 10:483-491

[16] Yang M., Zhang X., Vafai K., et al. (2003) High sensitivity Piezoresistive cantilever design and optimization for analyte-receptor binding. Micromech. Microeng., 13:64-72

[17] Yang S.M., Yin T.I. (2007) Design and analysis of piezoresistive microcantilever for surface stress measurement in biochemical sensor. Sensors Actuators B, 120: 736-744

[18] Ahmed A.S.M., Walied A.M., et al. (2010) Optimization of geometric Characteristics to improve sensing performance of MEMS Piezoresistive strain sensor. Micromech.Microeng., 20:015015

[19] Shi H.C., Fan S.C., et al. (2013) Design and FEM simulation study of the electro-thermal excitation resonant beam with slit-structure. Microsystem Technologies, 19 (7): 979-987

[20] Shi H.C., Fan S.C., et al. (2014) Theory and FEM simulation study of the double-clamped resonant beam with slit-structure. Microsystem Technologies, 20(6): 1141-1152.

[21] Bishop R.E.D., Jobnson D.C. (1956) Vibration Analysis Table. Cambridge University Press.

[22] Wilkinson P.R., Klug W.S., Leer B.V. and Gimzewski J.K. (2008) Nanomechanical Properties of Piezoresistive cantilevers:theory and experiment. Journal of Applied Physics 104:103527-7.

[23] Lobontiu N., Lupea L., Llic R., Craighead H.G. (2008) Modeling, design, and characterization of multisegment cantilevers for resonant mass detection. Journal of Applied Physics 103:064306-10.